www.elsevier.com/locate/yjssc

Local environments and transport properties of heavily doped strontium barium niobates $Sr_{0.5}Ba_{0.5}Nb_2O_6$

Riccardo Ottini, Cristina Tealdi, Corrado Tomasi, Ilenia. G. Tredici, Alessandro Soffientini, Ramón Burriel, Elías Palacios, Miguel Castro, Umberto Anselmi-Tamburini, Paolo Ghigna, Giorgio Spinolo

PII: S0022-4596(17)30395-X
DOI: https://doi.org/10.1016/j.jssc.2017.09.029
Reference: YJSSC19959

To appear in: *Journal of Solid State Chemistry*

Received date: 5 July 2017
Revised date: 27 September 2017
Accepted date: 29 September 2017

Cite this article as: Riccardo Ottini, Cristina Tealdi, Corrado Tomasi, Ilenia. G. Tredici, Alessandro Soffientini, Ramón Burriel, Elías Palacios, Miguel Castro, Umberto Anselmi-Tamburini, Paolo Ghigna and Giorgio Spinolo, Local environments and transport properties of heavily doped strontium barium niobates $Sr_{0.5}Ba_{0.5}Nb_2O_6$, *Journal of Solid State Chemistry,* https://doi.org/10.1016/j.jssc.2017.09.029

Local environments and transport properties of heavily doped strontium barium niobates $Sr_{0.5}Ba_{0.5}Nb_2O_6$.

Riccardo Ottini[†1], Cristina Tealdi[‡], Corrado Tomasi[§], Ilenia. G. Tredici[‡], Alessandro Soffientini[‡], Ramón Burriel[¶], Elías Palacios[¶], Miguel Castro[⌘], Umberto Anselmi-Tamburini[‡], Paolo Ghigna[‡], Giorgio Spinolo[‡].

[†] Department of Chemistry, University of Pavia (Italy).

[‡] Department of Chemistry, University of Pavia (Italy) and INSTM – Research Unit at University of Pavia, viale Taramelli 16, I27100 Pavia (Italy).

[§] CNR-ICMATE, Sede secondaria di Lecco, Via Previati 1E, I23900 Lecco (Italy)

[¶] Instituto de Ciencia de Materiales de Aragón (ICMA) and Departamento de Física de la Materia Condensada, CSIC–Universidad de Zaragoza, Pedro Cerbuna 12, 50009 Zaragoza, Spain

[⌘] Instituto de Ciencia de Materiales de Aragón (ICMA), CSIC–Universidad de Zaragoza, Campus Río Ebro, María de Luna, 3, 50018 Zaragoza, Spain

[1] Now at Dipartimento di Scienze Molecolari e Nanosistemi, University of Venice, Via Torino 155, I 30170 Venezia Mestre (Italy).

ABSTRACT

Undoped as well as K-doped (40%), Y-doped (40%), Zr-doped (10%), and Mo-doped (12.5%) strontium barium niobate $Sr_{0.5}Ba_{0.5}Nb_2O_6$ (SBN50) materials have been investigated to explore the effect of heavy doping on the structural and functional properties (thermo-power, thermal and electrical conductivities) both in the as prepared (oxidized) and reduced states.

For all materials, the EXAFS spectra at the Nb – K edge can be consistently analyzed with the same model of six shells around the Nb sites. Doping mostly gives a simple size effect on the structural parameters, but doping on the Nb sites weakens the Nb-O bond regardless of dopant size and charge. Shell sizes and Debye – Waller factors are almost unaffected by temperature and oxidation state, and the disorder is of static nature.

The functional effects of heavy doping do not agree with a simple model of hole or electron injection by aliovalent substitutions on a large band gap semiconductor.

With respect to the undoped samples, doping with Mo depresses the thermal conductivity by ~ 30%, Y doping enhances the electrical conductivity by an order of magnitude, while Zr doping increases the Seebeck coefficient by a factor of 2 - 3. Globally, the *ZT* efficiency factor of the K-, Y-, and Zr-doped samples is enhanced at least by one order of magnitude with respect to the undoped or Mo-doped materials.

INTRODUCTION

In comparison with thermo-electric (TE) materials containing elements such as Cd, Tl, Se, Te, Sb, Bi, the TE-oxides of alkali, alkali earth, and transition elements are generally cheaper and more health and environmental friendly, and the abundance of their constituent elements on Earth's crust is orders of magnitude higher. Among them, strontium barium niobates, $Sr_xBa_{1-x}Nb_2O_6$ (SBN) are interesting because of their low thermal conductivity, which is related to structural features[1,2] such as a basic open network of corner-sharing NbO_6 octahedra, incomplete occupancies of the (Sr, Ba) sites, as well as their nature of solid solutions ($Sr_xBa_{1-x}Nb_2O_6$ $x \approx 0.2$ – 0.62 at 1200 °C)[3].

Actually, SBNs have been investigated since long time not only as TE materials[4–10], but also for ferro-electricity[11–19] , dielectric properties[20–23], photocatalysis[24,25], and photorefractive, electro-optic, nonlinear optic, and fluorescence properties[26–32]. The structural aspects and their relation with the functional properties have been comprehensively discussed by Zhu et al[18] using a crystal-chemical model for the whole family of tetragonal bronzes. Fine details[33–41] of the basic tetragonal tungsten bronze crystal structure[1,2] are affected by Sr/Ba composition, thermal annealing, interaction with external oxygen[42], and the synthetic pathways[8,11–13,15,20–23,34–36,38,39,43–51].

According to literature, the band gap is ca. 3 eV and heavy chemical reduction is required to obtain an *n* - type thermoelectric material from SBNs. The Seebeck coefficient reaches 281 μV/ K at 930 K[5],[8] while a three orders of magnitude increase of the electrical conductivity has been related to a reduction of the binding energy of oxygen vacancies when approaching the ferroelectric transition[9]. The charge transport depends on the reduction temperature and

reduction degree, and a polaronic mechanism has been reported by several authors[6,52–54].

Doping is expected[55],[56] to further decrease thermal conductivity, but is mainly investigated in hopes of achieving good values of electrical conductivity (σ) and Seebeck coefficient (S), which are generally too low. However, only doping of SBN materials at low levels (few %) has been investigated largely[8,15,22,23,28,35,36,38,39,53,57–64], while it would be highly desirable to explore the feasibility and effectiveness of doping at high levels, when doping is expected to affect the whole band structure in addition to a simple injection of electrons or holes.

In this line, we have shown[65] that a solution chemistry approach is effective in producing SBN materials with nominal 0.5/0.5 (Sr/Ba) composition where 10 - 12.5 % of the Nb sites can be substituted by Zr and Mo, respectively, while the Sr cations can be substituted by K and Y at huge doping levels near 40%. We analyze in the present paper the effects of these doping levels on the local structure around Nb and on the transport properties (thermal and electrical conductivities and Seebeck coefficient) of SBN materials.

EXPERIMENTAL

Base-assisted co-precipitation from aqueous solutions of the single cations in the desired stoichiometry was used, followed by a heat treatment at 1150 °C. The cation ratios of starting solutions are $K_{0.2}Sr_{0.3}Ba_{0.5}Nb_2$, $Y_{0.25}Sr_{0.25}Ba_{0.5}Nb_2$, $Sr_{0.5}Ba_{0.5}Zr_{0.2}Nb_{1.8}$, $Sr_{0.5}Ba_{0.5}Mo_{0.25}Nb_{1.75}$. The single phase nature of the SBN materials has been verified by X-Ray powder diffraction for all dopants except Y, where a small amount of a foreign phase is formed and the final cation composition ($Y_{0.19}Sr_{0.27}Ba_{0.54}$) of the SBN material is close to that achieved with K-doping. The as-prepared samples are hereafter denoted as "oxidized" samples, while "reduced" samples have been prepared under strictly equal conditions followed by a further reduction step in a Spark Plasma Sintering (SPS) apparatus. Details on sample preparation have been reported previously[65].

X-Ray powder patterns have been taken[65] at room temperature with a Bruker D8 Advance diffractometer equipped with copper anode (Cu-K_α radiation, wavelength = 1.5418 Å) and graphite monochromator on the diffracted beam in the $15° \le 2\theta \le 90°$ range with 8 s counting time and 0.02° 2θ steps. For the Rietveld refinements we have used the MAUD program[66] starting from the assessed structure[1,2]. The general strategy was to refine first the instrumental, peak shape and crystallite size parameters, then lattice dimensions and atomic coordinates, and finally the occupancy factors. The lattice dimensions are in the ranges $12.46 \le a \le 12.56$ Å, $3.39 \le c \le 3.99$ Å depending on doping and redox state. We have verified[65] that Zr and Mo enter the Nb sites, while K and Y enter the sites of the divalent cations by replacing Sr. In particular, K replaces only the Sr of the A2 site (the site that is occupied jointly by Sr and Ba in undoped SNB50), while the A1 site is occupied only by the unsubstituted Sr: this is what expected from the ion radii of K^+ in the IX and XII coordination environments (1.55 and 1.64 Å,

respectively), that are much larger than those of Sr^{2+} (1.31 and 1.44 Å) and even larger than those of Ba^{2+} (1.47 and 1.61 Å)[67].

XAS spectra have been acquired in transmission mode at the LISA-BM08 beamline[68] (European Synchrotron Radiation Facility, ESRF, Grenoble, Fr) at the Nb–K edge. A Si(311) double crystal has been employed as monochromator and the harmonic rejection has been realized by Pd mirrors, having a cutoff energy of 20 keV. For the measurements, an amount of sample appropriate to give a unit jump in the absorption coefficient at the edge has been weighed, thoroughly mixed with cellulose and pressed to pellet.

The EXAFS has been extracted by using the ATHENA code[69] and the data analysis has been performed using the EXCURVE program[70]. Phases and amplitudes were calculated using the muffin-tin approximation, in the framework of the Hedin–Lundquist and Von Bart approximations for the exchange and ground state potentials, respectively[70]. This includes the effects of inelastic losses due to the electron inelastic scattering.

To check the reliability of the fits, different weighting schemes have been tested, thus finding that the fitting parameters are recovered within the errors. Multi-channel events are included in the Hedin–Lundquist approximation so that we have always found S_0^2 equal to one within the experimental errors, as expected: the S_0^2 parameter provides a measure of events like two-electron transitions where the energy difference between the photon and the photoelectron is so large that they are not seen in the spectrum.

The fitting model of the EXAFS is based on a simplified radial distribution around Nb, averaged over the two non-equivalent crystallographic sites of the P4bm tetragonal structure. In particular, the first, second, and third shells are made only of oxygen atoms at distances of about

1.9, 2.0, and 2.1 Å, respectively, in a distorted octahedral coordination. The forth shell, at about 3.4 Å is relative to the sites currently denoted as A1[2] and contains only Sr. The fifth shell at a larger distance is relative to the sites currently denoted as A2 sites and contains Sr and Ba. Then a shell at about 3.6 Å from the photo-absorber is due to the Nb atoms in the nearby octahedra. To avoid unnecessary correlation between the fitting parameters, and considering the quite scarce accuracy of EXAFS in the determination of coordination numbers, their values have been kept constant according to the composition of the samples and to the structural information from the scientific literature and from the refinement of powder diffraction data. Then, the shell parameters allowed to vary are only the distance from the photo-absorber and the thermal factor (DW, Debye-Waller).

Models with a larger number of shells, up to eight, were tried, but were found unreliable or did not provide meaningful additional information.

Note that, for all dopants except K, the scattering factors of the substituent and substituted ions are practically indistinguishable because of the equal number of electrons. This makes possible to identify substituent and substituted ions in the fit models and strongly simplifies *both* structural determinations (X-Ray powder diffraction and EXAFS). In other words, the scattering factor of Y is treated as equal to that of Sr, and the same applies to the scattering factors of Zr and Mo with respect to Nb. For the K case, the difference in scattering factor with respect to Sr cannot be ignored and the structure model is modified by placing the pertinent amount of K on the A2 sites, as said above.

Thermal conductivity, κ, was measured in the 30 – 120 °C on reduced samples by means of a PPMS (Quantum Design) device fitted with a thermal transport option, TTO, on cylindrical

samples (8 mm diameter, 2-3 mm thick) with gold plated electrodes stuck by a conductive paste. Heat was applied in order to create a temperature rise of 3% of the basic temperature between the two thermometer shoes. The sample thermal response is dynamically modeled by the TTO system and the thermal conductivity is directly calculated taking into account the applied power, resulting ΔT, and sample geometry. Using a standard sample, the estimated accuracy is about ± 5%.

For the electric transport properties (σ and S), the reduced samples have been used in form of Pt-sputtered cylindrical samples. The electrical conductivity measurements have been obtained with a two-probe cell equipped with Pt electrodes using a MaterialMates mod. 7260 Frequency Response Analyzer. Frequency – independent pure ohmic impedance was always found. The Seebeck coefficient (S) has been determined from the slope of the $\Delta V/\Delta T$ plots using a home-made apparatus. In all cases the measurements have been made under a nitrogen atmosphere to prevent re-oxidation. The electrical conductivity of oxidized samples was always found at least eight orders of magnitude lower than that of the corresponding reduced samples and therefore their electrical properties have not been further investigated.

RESULTS AND DISCUSSION

Fig. 1 shows the thermal conductivity of reduced SNB materials and its changes with doping. Doping depresses the thermal conductivity, but the trends suggest that above 150 C the Y-, Zr-, and K-doped samples are not very far from the undoped SBN. The Mo-doped sample not only shows the lowest conductivity (about 30% better than the undoped sample), but also shows weaker temperature dependence than the other dopants. The electronic contribution to thermal conductivity is almost negligible, as shown both by the satisfactorily agreement with published data on oxidized and undoped single crystals with nearby compositions (Sr:Ba = 52:48)[10] and by applying the Wiedemann - Franz law to the data of Fig. 1.

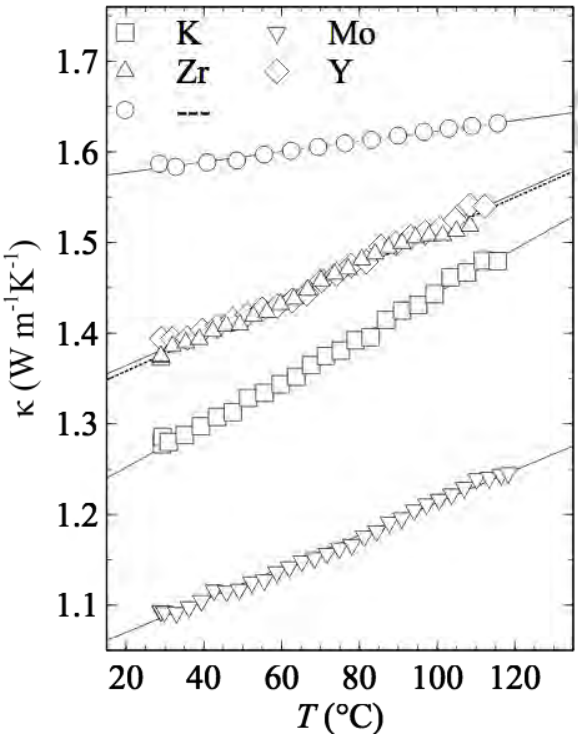

Fig. 1. Thermal conductivity of reduced SBN materials. The straight lines are linear fits.

The electrical conductivity of reduced samples (Fig. 2), as said, is more than eight orders of magnitude above the values for the oxidized samples[65]. When reduced under equal conditions, the doped samples show conductivity enhancements with respect of the undoped materials. With

Y, the enhancement amounts to more than one order of magnitude, while Mo doping is practically ineffective. The conduction mechanism of a non-degenerate semiconductor must follow a linear trend in Arrhenius coordinates, but only the Mo and K dopants reasonably agree with this behavior (Fig. 3) in the whole temperature range. The deviations from Arrhenius behavior found with the other samples are probably due to a change with temperature of the conduction mechanism.

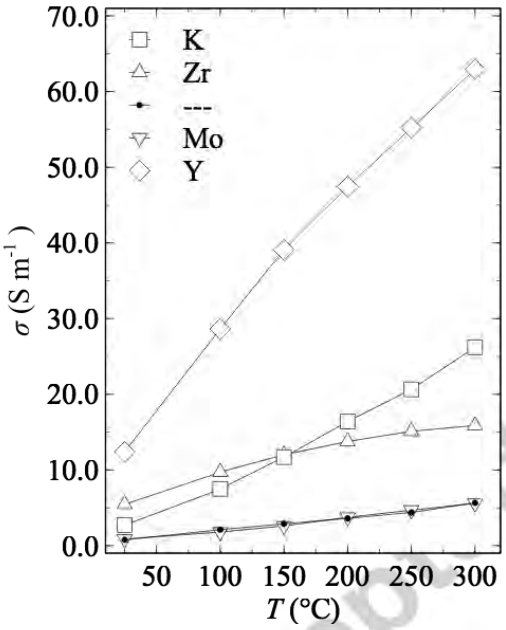

Fig. 2. Electrical conductivity of reduced SBN materials. The lines are guides to eye.

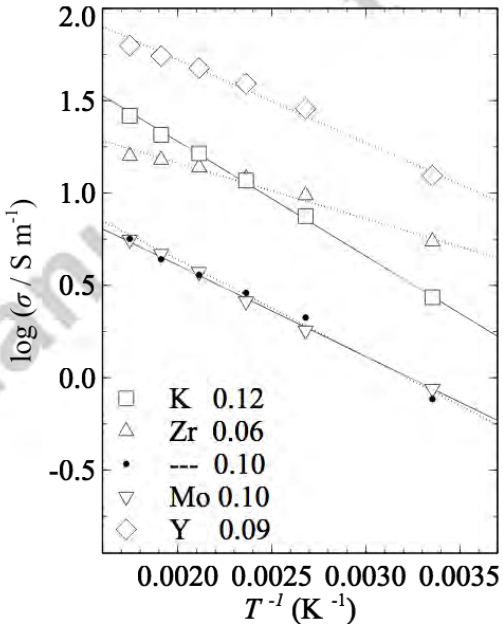

Fig. 3. Arrhenius plots of the data of the previous figure. The numbers are the activation energies of the fits (in eV).

The Seebeck coefficient is always negative and is generally enhanced by doping (Fig. 4). Quantitatively, the effect is very small with Mo but significant with K, Y, and Zr (from least to biggest effect). Zr doping significantly increases also the temperature dependence. With this dopant, starting at around 100 °C, the Seebeck coefficient distinctively agrees (Fig. 5) with the model of a non-degenerate semiconductor[7,71,72], where S increases linearly with $\ln(N_c)$, N_c is the effective density of states in the conduction band, and its temperature dependence is

$N_c \propto T^{3/2}$. For the other dopants, deviation from the expected behavior suggests that, also for the Seebeck coefficient, the temperature increase produces a change in transport mechanism: this is most clearly seen in the Y-doped material.

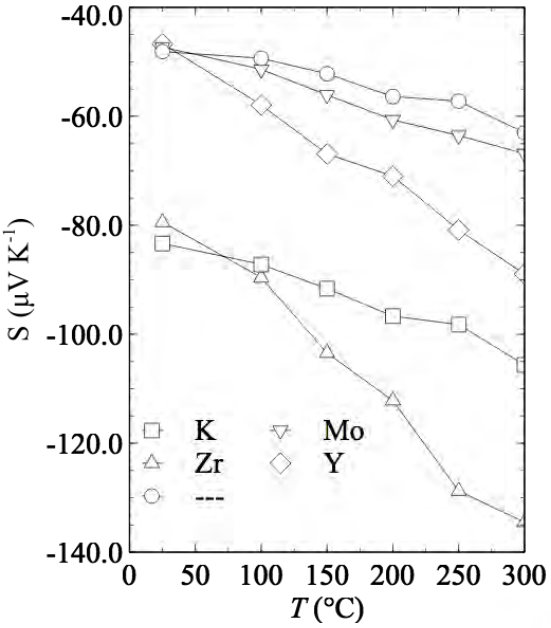

Fig. 4. Seebeck coefficient of reduced SBN materials. The lines are guides to eye.

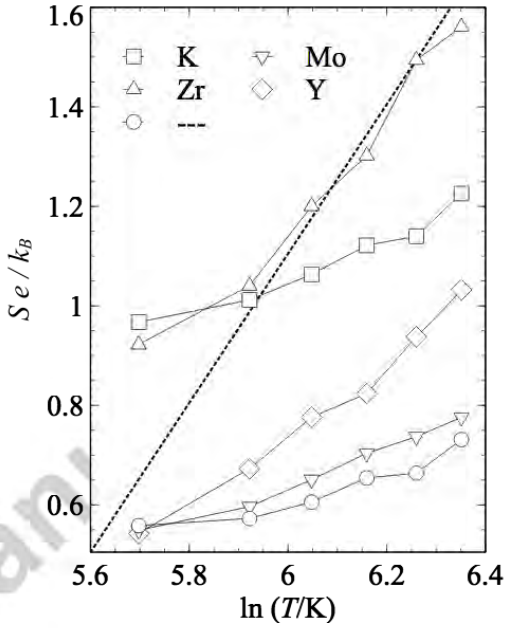

Fig. 5. Seebeck coefficient of reduced SBN materials. The dashed line corresponds to the linear $S\ vs\ \frac{3}{2}\ln T$ trend.

Let us now discuss the structural changes. Strongly simplifying a complex topic, the corner-sharing NbO_6 octahedra of the SBN structure[1,2] are arranged in rows running along the *c* axis and are also connected to each other in one-octahedron-thick layers parallel to the *ab* plane, as shown in Fig. 6. In the oxygen channels between the rows, there are two main sites (A1 and A2) for the alkali earth cations. Both sites have high (12 and 9, respectively) coordination, fairly large cation – oxygen distances, and largely incomplete occupancies. In undoped SBNs, the A1 sites contain only Sr, while Sr and Ba share the A2 sites, and the amount of Sr lying on A1 or A2 depends on the Sr/Ba composition.

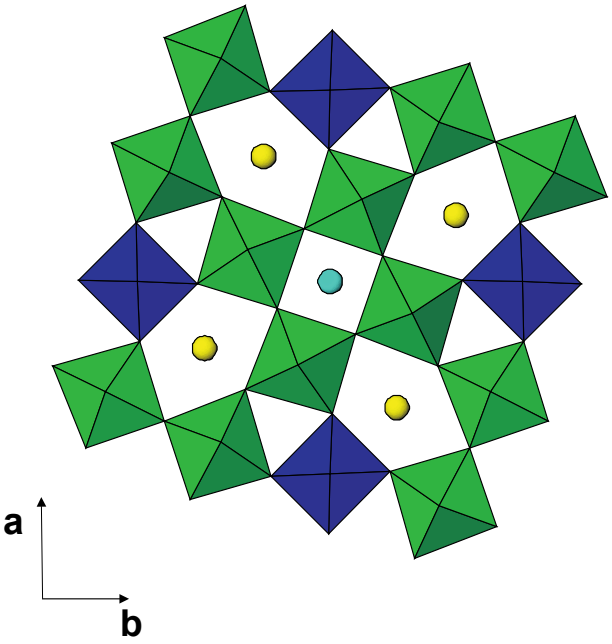

Fig. 6. The tetragonal (|**a**|=|**b**|) tungsten bronze structure of the SBNs[1,2] is made of an open network of corner – sharing NbO_6 octahedra arranged in columns running along the *c* axis. Two different sets of symmetry - equivalent octahedra are marked in green and dark blue. The columns of the green set are in turn arranged into larger structural units made of four columns. The unit cell contains five ANb_2O_6 formulas (A = divalent cation, Sr or Ba) and its length along **c** corresponds to one (slightly tilted) octahedron. The space group is *P4bm* (No 100 of the *International Tables*[73]). Cyan and yellow spheres mark the A1 and A2 sites for the divalent cations that are respectively along the square channels (Wyckoff position 2a) and irregular pentagonal channels (Wyckoff position 4c).

Doping strongly affects (Fig. 7) the distribution of the cations and the effect depends on the size of the dopant but also on the site where the substitution occurs. As typically done in solid-state chemistry, a size effect on structural parameters can be discussed using a size discrepancy parameter (*D*):

$$D = \frac{r_0 - r'}{r_0}; \quad r' = x \cdot r + (1 - x) \cdot r_0$$

where *x* is the mole fraction of the dopant, r_0 is the size of the replaced ion, while *r* is the size of the replacing ion[67]. Our results show that the nature of the dopant generally affects the structural parameters in the two clearly different ways: a) an almost linear trend *vs D* for all samples, the undoped one included or b) an analogous linear trend when the substitution regards the A sites, coupled with shifts of the same sign with respect to the undoped sample when the substitution regards the Nb sites. The first behavior is reasonably indicative of a simple ion size effect and concerns the *c* lattice constant[65] and most parameters of the local structure around

Nb, as discussed below. The second behavior is indicative of a weakening of the Nb – O bonds and concerns the *a* lattice constant[65] as well as the A1/A2 occupancy ratio (Fig. 7).

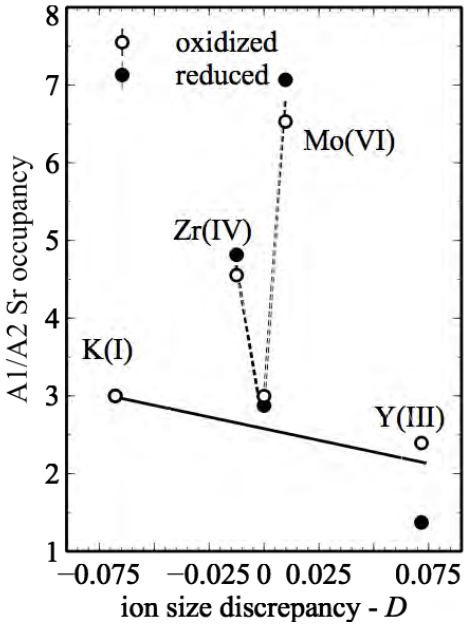

Fig. 7. Sr occupancy of the A1 and A2 sites. Ba enters only the A2 site, Sr enters both A1 and A2 sites. The difference in scattering factors between Sr and Y has been neglected. For the K-doped samples, substitution occurs only on the A2 sites, the difference in scattering factors is considered, and K and Sr occupancies of the A2 sites are added when evaluating the occupancy ratio.

The local structure around Nb has been investigated with EXAFS at the Nb-K edge. Fig. 8 shows an example of the EXAFS signal with its fit according to the six shells model described in the experimental section. The peaks in the FT (Fourier transform, right part) show that the cation shells (next nearest shells) affect the EXAFS only above 3 Å. With all samples, the local environments of the Nb sites can be consistently analyzed with these shells, independently of temperature, nature of the dopant and oxidation state of the sample.

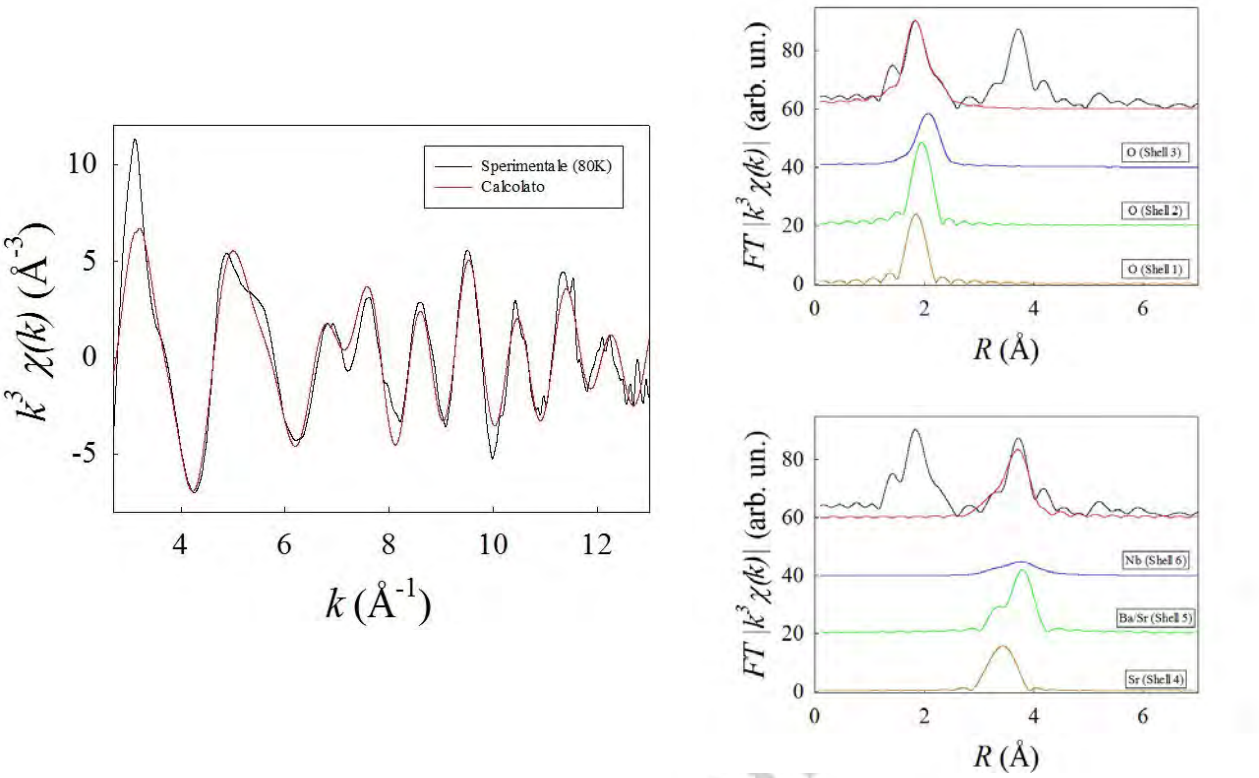

Fig. 8. EXAFS of the undoped oxidized sample at 80 K (left part) and (right part) its Fourier transform with the components due (upper panel) to the first, second and third Nb-O shells and (lower panel) to the Nb-A1, Nb-A2 and Nb-Nb shells.

Concerning the nature of dopant, the regular and roughly linear trend with *D* is stronger than the concurrent trend due to doping on Nb sites. Fig. 9 shows the trend of the shell sizes: going from K to Y, the changes of the respective parameters amount to 1.5 – 5% depending on the parameter. A similar trend can be seen also for the DW factors of the third oxygen shell and the Nb-A1 and Nb-A2 shells (Fig. 10).

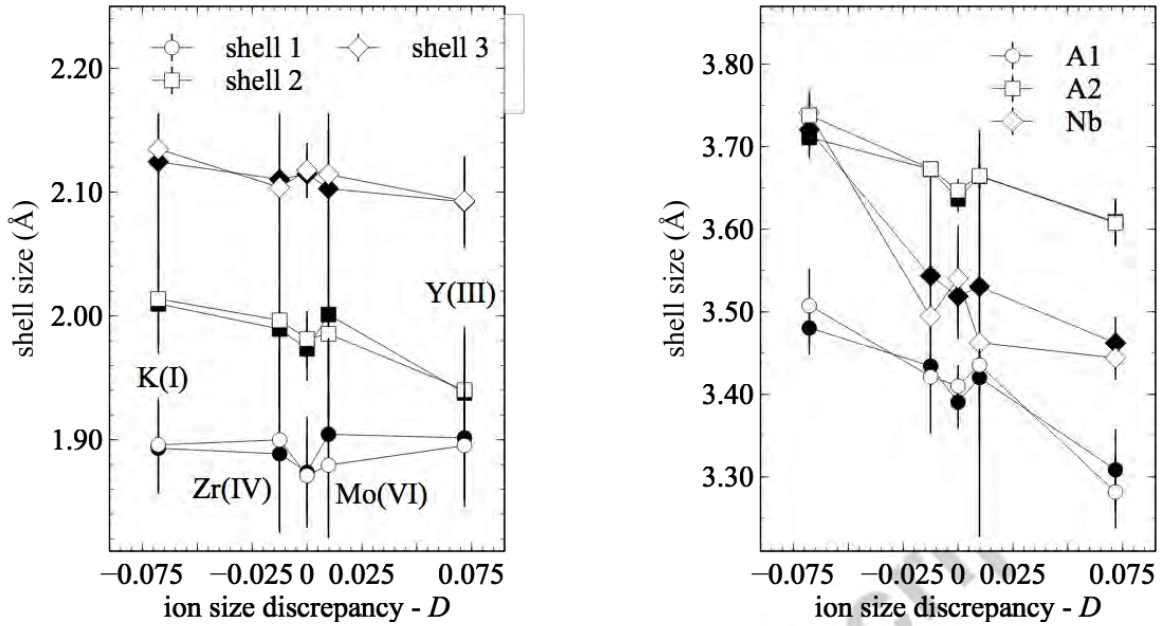

Fig. 9. Sizes of the Nb-O shells (left panel) and the Nb-A1, -A2 or –Nb shells (right panel) for various dopants at 80 K. Open and filled symbols refer to oxidized and reduced samples.

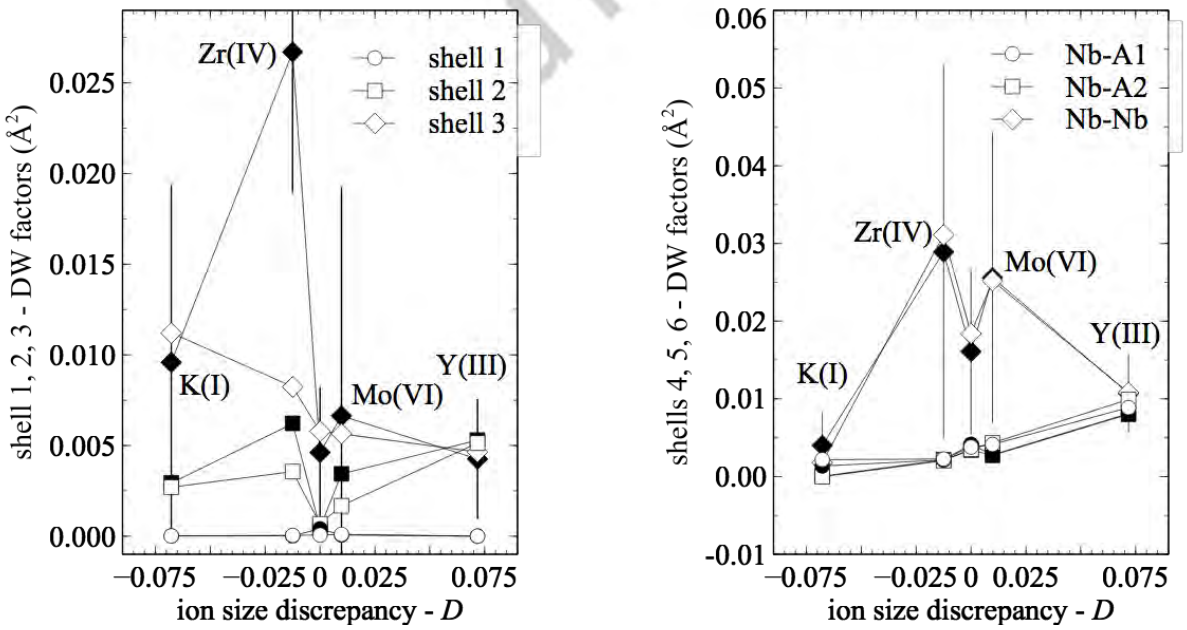

Fig. 10. DW factors of various shells for various dopants at 80 K. Open and filled symbols refer to oxidized and reduced samples. For better clarity, in the right panel the error bars are shown only for the Nb-Nb shell of the reduced sample

Almost generally, temperature does not significantly affect shell sizes and DW factors: examples are given in Fig. 11. Static disorder always predominates over thermal disorder, a result that is in full agreement with the very low experimental values of the thermal conductivity and can be related to the general features of the structure. However, we warn that the result can be due also to the data analysis procedure that groups various sub-shells into fewer composite shells.

Finally, the oxidation state of the sample does not generally affect in a significant way the structural parameters, lattice constants, A1/A2 occupancy, sizes, and DW factors of the various shells.

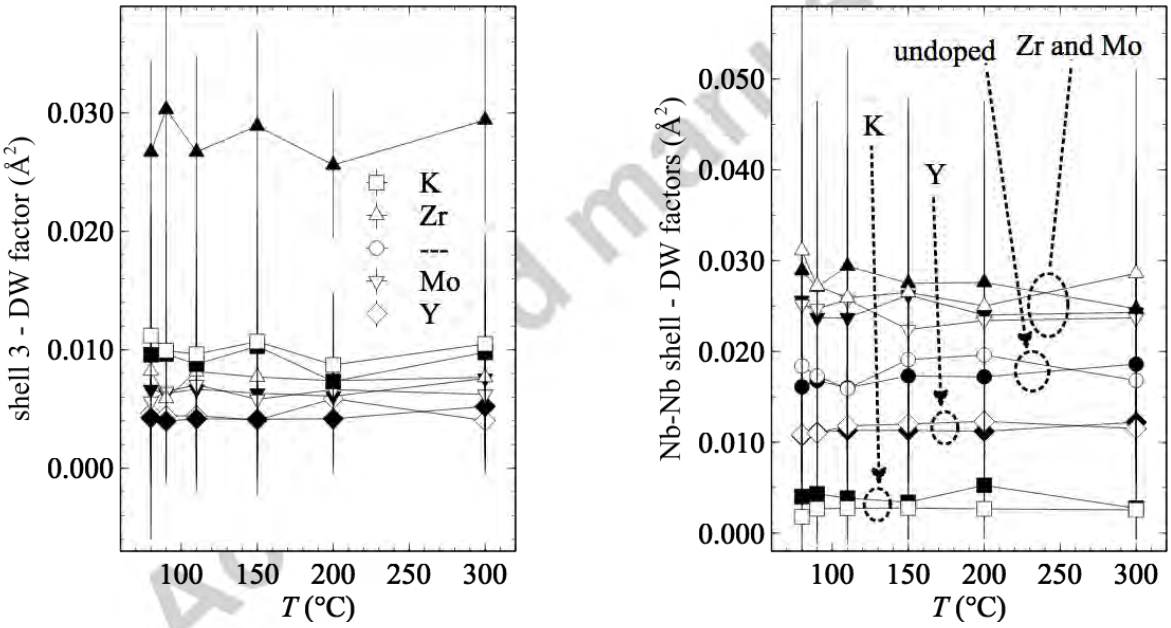

Fig. 11. Trend with temperature of the DW factors of the third Nb-O shell (left panel) and the Nb-Nb shell (right panel). Open and filled symbols refer to oxidized and reduced samples.

There are few exceptions to these general trends.

a) Differently from the other dopants and from the undoped case, the K-doped samples show Nb-A2 and Nb-Nb shell sizes practically equal to each other (right panel of Fig. 9), while the DW

factors of all the Nb-cation shells (see right panel of Fig. 11 for an example) are zero to within the experimental errors. All these features are unaffected by changes of temperature and oxidation state. A reasonable explanation relies in the large size of the K^+ ion and the fact that it replaces the Sr on the A2 site. Clearly, this dopant strains the structure much more than the other dopants and gives rise to a stronger correlation between the displacements of Nb and the ions in the A2 site.

b) A small and not fully reliable sign of thermal disorder can be seen on the DW factors of the Nb-A1 and Nb-A2 shells of undoped, Zr-doped, or Mo-doped samples.

c) A strong effect of chemical reduction can be seen on the DW factor of the third Nb-O shell for the Zr-doped sample (left panel of Fig. 10). The effect can be seen in all temperature range.

d) The DW factors of the Nb-Nb shell (right panel of Fig. 11) depend on nature of the dopant in a distinctive way, not found for the other structural parameters. Both dopants replacing Sr (K and Y) reduce the DW factors with respect to the undoped samples and do not show the general linear trend indicative of a simple size effect. Incidentally, also the dopants on the Nb sites (Zr and Mo) affect the DW factors of the Nb-Nb shell in a concordant way, now increasing the parameter values: this trend, however, is typical of other structural parameters and can be similarly explained by a weakening of the Nb-O bonds, as said.

Conclusions

The injection of mobile carriers with huge doping of the SNB structure can be discussed making reference to a simple two-bands model and two mechanisms. The first one is the direct compensation of the charged substitutional defects with mobile electrons or holes. Writing the reactions with a doping oxide entering and a regular oxide leaving the structure, just to keep simple the notation, these are:

$$K_2O + 2\,Sr_{Sr}^{x} + \tfrac{1}{2}\,O_2(gas) \longrightarrow 2\,K'_{Sr} + 2\,h^{\bullet} + 2\,SrO$$

$$Y_2O_3 + 2\,Sr_{Sr}^{x} \longrightarrow 2\,Y_{Sr}^{\bullet} + 2\,e' + \tfrac{1}{2}\,O_2(gas) + 2\,SrO$$

$$2\,ZrO_2 + 2\,Nb_{Nb}^{x} + \tfrac{1}{2}\,O_2(gas) \longrightarrow 2\,Zr'_{Nb} + 2\,h^{\bullet} + Nb_2O_5$$

$$2\,MoO_3 + 2\,Nb_{Nb}^{x} \longrightarrow 2\,Mo_{Nb}^{\bullet} + \tfrac{1}{2}\,O_2(gas) + 2\,e' + Nb_2O_5$$

With the other mechanism, the substitutional defects are balanced by oxygen defects that in turn can produce the mobile carriers by equilibrium with the external atmosphere. For doping on the Sr sites this is:

$$K_2O + 2\,Sr_{Sr}^{x} \longrightarrow 2\,K'_{Sr} + V_O^{\bullet\bullet} + 2\,SrO \quad \text{followed by} \quad V_O^{\bullet\bullet} + \tfrac{1}{2}\,O_2(gas) \rightleftarrows O_O^{x} + 2\,h^{\bullet} \text{ or}$$

$$Y_2O_3 + 2\,Sr_{Sr}^{x} \longrightarrow 2\,Y_{Sr}^{\bullet} + O_i'' + + 2\,SrO \quad \text{followed by} \quad O_i'' \rightleftarrows \tfrac{1}{2}\,O_2(gas) + 2\,e'$$

Doping on the Nb sites can be treated in a closely similar way.

According to these mechanisms, doping with lower valence or higher valence cations produces opposite effects for what concerns the sign of the carriers, injected either directly or through reduction or oxidation equilibria. This simple scheme also suggests the appealing possibilities of

a) preparing performing *n*-type conductors without the need of high temperature treatments under low oxygen partial pressures and b) achieving both *n*-type and *p*-type SBN conductors using different dopants.

The most striking result of the present investigation of heavy doping of the SNB structure is that the actual effects of doping are remarkably different from all these naïve expectations.

Aliovalent dopants of opposite charges do not show the expected opposite effects, particularly on carrier injection. Even when pushed to 10-12 % of the Nb sites or to a huge 40% of the Sr sites, doping produces only insulating materials and reduction is always required to produce electrically conductive materials. Then, both higher or lower valence dopants produce *n*-type conductors and enhance the electrical properties with respect to the undoped material-.

There is a negligible effect of doping concerning the charge state of Nb: as previously reported[65], it remains +5 irrespective of nature of dopant, temperature and chemical reduction treatment. Fine differences in intensity of a pre-edge feature of the XAS spectrum indicate that doping affects the density of empty Nb 4d states in a way that is again in disagreement with the simple picture of aliovalent doping. A higher-valence cation is expected to increase the spectral weight and a lower-valence cation is expected to decrease the spectral weight. Experimentally we found that the Y-doped sample shows higher intensity, and the Zr-doped sample shows lower intensity, but also that the K- and Mo-doped samples are similar to the undoped sample. We incidentally remind (see above) that the Zr-doped sample is particular in showing a clear structural effect of chemical reduction, i.e. a particularly large DW factor of its 3rd Nb-O shell in all temperature range.

The huge doping achieved does not produce dramatic modifications of the SBN structure and

finer changes of structural parameters do not show opposite effects changing the sign of the charge of the substitutional defects. In most cases, these changes are directly explained by a simple ion size effect, while doping on the Nb sites changes the *a* lattice constant[65] and the A1/A2 occupancy ratio in the same direction with differently charged dopants, a result that can be explained as a weakening of the Nb – O bonds.

With a single exception for the DW factor of the third Nb-O shell of the Zr-doped sample, the structural parameters are not remarkably affected by chemical reduction.

The O shells do not generally show marked difference with nature of dopant, which gives further evidence that the substitutional defects are not stoichiometrically compensated by oxygen defects.

A reasonable explanation of these aspects is that the substitutional defects give rise to shallow levels and are therefore unable to inject mobile carriers either directly or through oxygen defects.

Jumps of more than eight orders of magnitude in electrical conductivity are obtained by chemical reduction of the different samples under equal conditions: this indicates that the onset of conductivity is entirely due to oxygen vacancies that form under low oxygen partial pressure while place, size and charge of the dopants seemingly play a minor role.

While huge doping with aliovalent cations does not give the desired improvements of the basic strategy towards performing TE materials of the SBN family, it is anyway able to produce enhancements of the order of a power of ten.

The smallest effect is on the thermal conductivity: all dopants decrease the property, but the change is at most 30 % with Mo-doping.

Mo doping does not affect significantly the electrical conductivity of the reduced samples, while the other dopants produce an increase of 10 times (Y) or 3-5 times (K and Zr).

The Seebeck coefficient is always negative and enhanced by doping. The increase is very small with Mo, better with K and Y, best with Zr, when doping significantly increases also the temperature dependence.

Finally, the power factor is clearly better (one order of magnitude or more) for Y -, K –, and Zr doped samples and this trend is closely followed by the *ZT* coefficient (Fig. 12). Power factor and *ZT* are almost unchanged by Mo-doping.

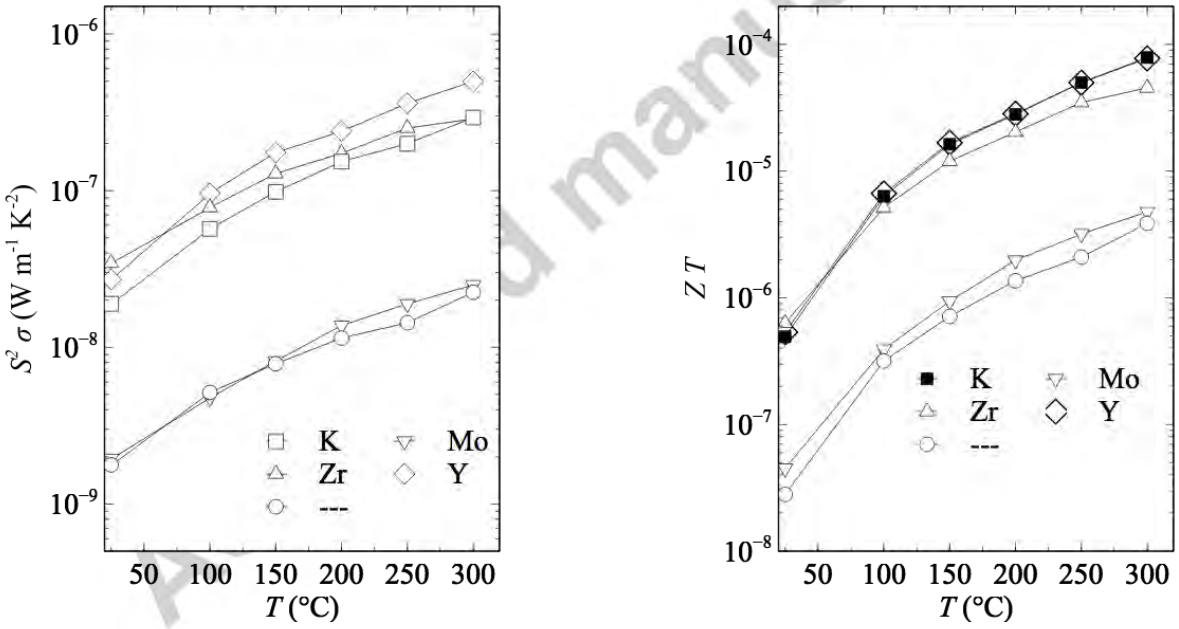

Fig. 12. Effect of doping on power factor (left) and the *ZT* thermoelectric efficiency parameter (right) of the various samples, after reduction. To compare the *ZT* coefficient of the various materials in a wider temperature range, the thermal conductivity data (see Fig. 1) have been linearly extrapolated to 300 °C.

ACKNOWLEDGMENTS

This work has been supported by the "Materiali Avanzati" Program (Projet code 2012-0815) of the Cariplo foundation (Milano, Italy). BM08 (LISA)@ESRF is acknowledged for the provision of beam-time, travel and accommodation expenses (Exp. HC-1582). Thanks are given to Dr Francesco d'Acapito for considerable help during experiment setup and collecting EXAFS data and to Ana Arauzo and Enrique Guerrero for help in collecting thermal conductivity data.

REFERENCES

[1] P.B. Jamieson, S.C. Abrahams, J.L. Bernstein, Ferroelectric Tungsten Bronze-Type Crystal Structures. I. Barium Strontium Niobate $Ba_{0.27}Sr_{0.75}Nb_2O_{5.78}$, J. Chem. Phys. 48 (1968) 5048–5057. doi:10.1063/1.1668176.

[2] M.P. Trubelja, E. Ryba, D.K. Smith, A study of positional disorder in strontium barium niobate, J. Mater. Sci. 31 (1996) 1435–1443. doi:10.1007/BF00357850.

[3] C. Nikasch, M. Göbbels, Phase relations and lattice parameters in the system SrO–BaO–Nb_2O_5 focusing on SBN ($Sr_xBa_{1-x}Nb_2O_6$), J. Cryst. Growth. 269 (2004) 324–332. doi:10.1016/j.jcrysgro.2004.04.037.

[4] K. Wagner, E. Hegenbarth, Thermal-Conductivity of Strontium-Barium-Niobat Under High-Pressure And, Ferroelectr. Lett. Sect. 16 (1993) 95–102. doi:10.1080/07315179308204265.

[5] S. Lee, R.H.T. Wilke, S. Trolier-McKinstry, S. Zhang, C.A. Randall, $Sr_xBa_{1-x}Nb_2O_{6-\delta}$ Ferroelectric-thermoelectrics: Crystal anisotropy, conduction mechanism, and power factor., Appl. Phys. Lett. 96 (2010) 031910. doi:10.1063/1.3291563.

[6] S. Lee, S. Dursun, C. Duran, C.A. Randall, Thermoelectric power factor enhancement of textured ferroelectric $Sr_xBa_{1-x}Nb_2O_{6-\delta}$ ceramics, J. Mater. Res. null (2011) 26–30. doi:10.1557/jmr.2010.78.

[7] S. Lee, J.A. Bock, S. Trolier-McKinstry, C.A. Randall, Ferroelectric-thermoelectricity and Mott transition of ferroelectric oxides with high electronic conductivity, J. Eur. Ceram. Soc. 32 (2012) 3971–3988. doi:10.1016/j.jeurceramsoc.2012.06.007.

[8] C.S. Dandeneau, T.W. Bodick, R.K. Bordia, F.S. Ohuchi, Thermoelectric Properties of Reduced Polycrystalline $Sr_{0.50}Ba_{0.50}Nb_2O_6$ Fabricated Via Solution Combustion Synthesis, J. Am. Ceram. Soc. 96 (2013) 2230–2237. doi:10.1111/jace.12319.

[9] G.D. Mahan, J.O. Sofo, The Electrical Conductivity of Strontium-Barium Niobate,

J. Electron. Mater. 42 (2013) 1375–1376. doi:10.1007/s11664-012-2248-6.
[10] C.L. Choy, W.P. Leung, T.G. Xi, Y. Fei, C.F. Shao, Specific heat and thermal diffusivity of strontium barium niobate ($Sr_{1-x}Ba_xNb_2O_6$) single crystals, J. Appl. Phys. 71 (1992) 170–173. doi:10.1063/1.350732.
[11] Y.S. Yang, M.K. Ryu, H.J. Joo, S.H. Lee, S.J. Lee, K.Y. Kang, M.S. Jang, Ferroelectricity and electronic defect characteristics of *c*-oriented $Sr_{0.25}Ba_{0.75}Nb_2O_6$ thin films deposited on Si substrates, Appl. Phys. Lett. 76 (2000) 3472–3474. doi:10.1063/1.126681.
[12] S.T. Liu, R.B. Maciolek, Rare-earth-modified $Sr_{0.5}Ba_{0.5}Nb_2O_6$ ferroelectric crystals and their applications as infrared detectors, JEM. 4 (1975) 91–100. doi:10.1007/BF02657838.
[13] G. Mattausch, T. Felsner, E. Hegenbarth, B. Kluge, S. Sahling, Glassy properties of the relaxor ferroelectric strontium barium niobate at low temperatures, Phase Transit. 59 (1996) 189–223. doi:10.1080/01411599608220044.
[14] S. Murty, K. Murthy, G. Padmavathi, A. Bhanumathi, K. Murty, Relaxor Studies of Na, Fe and Mg Doped Sbn Ceramics, I E E E, New York, 1992.
[15] I. Bhaumik, S. Ganesamoorthy, R. Bhatt, N. Subramanian, A.K. Karnal, P.K. Gupta, S. Takekawa, K. Kitamura, Influence of cerium doping on the dielectric relaxation of $Sr_{0.75}Ba_{0.25}Nb_2O_6$ single crystal grown by the double crucible Stepanov technique, J. Alloy. Compd. 621 (2015) 26–29. doi:10.1016/j.jallcom.2014.09.196.
[16] S.H. Kshirsagar, S.R. Jigajeni, A.N. Tarale, D.J. Salunkhe, P.B. Joshi, Investigations on Fe-doped strontium barium niobate, single phase ferroelectric and magnetodielectric compounds, J. Adv. Dielectr. 5 (2015) 1550001. doi:10.1142/S2010135X15500010.
[17] C.M. Dudhe, S.B. Nagdeote, C.P. Chaudhari, Ferroelectric Domains in Sr0.5Ba0.5Nb2O6 (SBN50) at Nanolevel, Ferroelectrics. 482 (2015) 104–112. doi:10.1080/00150193.2015.1057080.
[18] X. Zhu, M. Fu, M.C. Stennett, P.M. Vilarinho, I. Levin, C.A. Randall, J. Gardner, F.D. Morrison, I.M. Reaney, A Crystal-Chemical Framework for Relaxor versus Normal Ferroelectric Behavior in Tetragonal Tungsten Bronzes, Chem. Mat. 27 (2015) 3250–3261. doi:10.1021/acs.chemmater.5b00072.
[19] G.H. Olsen, U. Aschauer, N.A. Spaldin, S.M. Selbach, T. Grande, Origin of ferroelectric polarization in tetragonal tungsten-bronze-type oxides, Phys. Rev. B. 93 (2016) 180101. doi:10.1103/PhysRevB.93.180101.
[20] Y. Liu, C.W. Ong, C.L. Choy, P.W. Chan, Dielectric and ferroelectric properties of pulsed laser deposited strontium barium niobate thin films, in: S.B. Desu, R. Ramesh, B.A. Tuttle, R.E. Jones, I.K. Yoo (Eds.), Ferroelectric Thin Films V, Materials Research Soc, Pittsburgh, 1996: pp. 131–136.
[21] G. Chen, B. Qi, Microstructure and dielectric properties of CBS glass-doped

$Sr_{0.5}Ba_{0.5}Nb_2O_6$ ceramic system, J. Mater. Sci.-Mater. Electron. 20 (2009) 248–252. doi:10.1007/s10854-008-9711-4.

[22] G. Stanciu, A. Achim, N.D. Scarisoreanu, V. Ion, R. Birjega, E. Andronescu, M. Dinescu, Synthesis of calcium doped strontium barium niobate ceramic samples, Optoelectron. Adv. Mater.-Rapid Commun. 9 (2015) 720–723.

[23] T.S. Velayutham, N.I.F. Salim, W.C. Gan, W.H. Abd. Majid, Effect of cerium addition on the microstructure, electrical and relaxor behavior of Sr0.5Ba0.5Nb2O6 ceramics, J. Alloys Comp. 666 (2016) 334–340. doi:10.1016/j.jallcom.2015.12.248.

[24] D. Fan, R. Chong, F. Fan, X. Wang, C. Li, Z. Feng, A tetragonal tungsten bronze-type photocatalyst: Ferro-paraelectric phase transition and photocatalysis, Chin. J. Catal. 37 (2016) 1257–1262. doi:10.1016/S1872-2067(15)61126-3.

[25] D. Fan, J. Zhu, X. Wang, S. Wang, Y. Liu, R. Chen, Z. Feng, F. Fan, C. Li, Dual Extraction of Photogenerated Electrons and Holes from a Ferroelectric Sr0.5Ba0.5Nb2O6 Semiconductor, ACS Appl. Mater. Interfaces. 8 (2016) 13857–13864. doi:10.1021/acsami.6b00809.

[26] S. Sakamoto, T. Yazaki, Anomalous electro-optic properties of ferroelectric strontium barium niobate and their device applications, Appl. Phys. Lett. 22 (1973) 429–431. doi:10.1063/1.1654700.

[27] M. Ewbank, R. Neurgaonkar, W. Cory, J. Feinberg, Photorefractive Properties of Strontium-Barium Niobate, J. Appl. Phys. 62 (1987) 374–380. doi:10.1063/1.339807.

[28] R. Baetzold, Calculations of Defect Properties Important in Photorefractive $Sr_{0.6}Ba_{0.4}Nb_2O_6$, Phys. Rev. B. 48 (1993) 5789–5796. doi:10.1103/PhysRevB.48.5789.

[29] T. Kume, K. Nonaka, M. Yamamoto, Wavelength-multiplexed holographic recording in cerium doped strontium barium niobate by using tunable laser diode, Jpn. J. Appl. Phys. 35 (1996) 448–453. doi:10.1143/JJAP.35.448.

[30] M. Daldosso, A. Speghini, P. Ghigna, M. de la O. Ramirez, D. Jaque, L.E. Bausa, J.G. Sole, M. Bettinelli, Lanthanide doped strontium barium niobate: Optical spectroscopy and local structure at the impurity sites, J. Alloy. Compd. 451 (2008) 12–17. doi:10.1016/j.jallcom.2007.04.119.

[31] P. Molina, H. Loro, S. Alvarez-Garcia, L.E. Bausa, E. Martin Rodriguez, O. Guillot-Noel, P. Goldner, M. Bettinelli, P. Ghigna, J. Garcia Sole, Site location and crystal field of Nd^{3+} ions in congruent strontium barium niobate, Phys. Rev. B. 80 (2009) 054111. doi:10.1103/PhysRevB.80.054111.

[32] Y. Zhou, Correlated Oxides: Material Physics and Devices, Doctoral Dissertation, Harvard University, 2015. https://dash.harvard.edu/handle/1/17464472 (accessed June 14, 2016).

[33] T.S. Chernaya, B.A. Maksimov, I.V. Verin, L.I. Ivleva, V.I. Simonov, Crystal

structure of $Ba_{0.39}Sr_{0.61}Nb_2O_{5.78}$ single crystals, Crystallogr. Rep. 42 (1997) 375–380.

[34] T.S. Chernaya, B.A. Maksimov, I.A. Verin, L.I. Ivleva, V.I. Simonov, Refinement of the single-crystal structure of $Sr_{0.61}Ba_{0.39}Nb_2O_6$: Ce, Crystallogr. Rep. 43 (1998) 986–990.

[35] T.S. Chernaya, B.A. Maksimov, T.R. Volk, L.I. Ivleva, V.I. Simonov, Atomic structure of $Sr_{0.75}Ba_{0.25}Nb_2O_6$ single crystal and composition-structure-property relation in $(Sr,Ba)Nb_2O_6$ solid solutions, Phys. Solid State. 42 (2000) 1716–1721. doi:10.1134/1.1309457.

[36] T.S. Chernaya, T.R. Volk, B.A. Maksimov, M.K. Blomberg, L.I. Ivleva, I.A. Verin, V.I. Simonov, X-ray diffraction study of cerium-and thulium-doped $(Sr,Ba)Nb_2O_6$ single crystals, Crystallogr. Rep. 48 (2003) 933–938. doi:10.1134/1.1627434.

[37] J. Schefer, D. Schaniel, V. Petricek, T. Woike, A. Cousson, M. Woehlecke, Reducing the positional modulation of NbO(6)-octahedra in Sr(x)Ba(1-x)Nb(2)O(6) by increasing the barium content: A single crystal neutron diffraction study at ambient temperature for x=0.61 and x=0.34, Z. Kristall. 223 (2008) 399–407. doi:10.1524/zkri.2008.0040.

[38] G.M. Kuz'micheva, L.I. Ivleva, I.A. Kaurova, V.B. Rybakov, Structural peculiarities and point defects of undoped and Cr- and Ni-doped $Sr_{0.61}Ba_{0.39}Nb_2O_6$ crystals, Acta Mater. 70 (2014) 208–217. doi:10.1016/j.actamat.2014.02.012.

[39] I.A. Kaurova, G.M. Kuz'micheva, L.I. Ivleva, V.V. Chernyshev, V.B. Rybakov, E.N. Domoroshchina, X-ray powder diffraction methods for the determination of composition and structural parameters of Cr- and Ni-doped $Sr_{0.61}Ba_{0.39}Nb_2O_6$ crystals, J. Alloy. Compd. 638 (2015) 159–165. doi:10.1016/j.jallcom.2015.03.080.

[40] S. Chillal, D. Koulialias, S.N. Gvasaliya, R.A. Cowley, L.I. Ivleva, S.G. Lushnikov, A. Zheludev, Phase transition of chemically doped uniaxial relaxor ferroelectric, J. Phys.-Condes. Matter. 27 (2015) 435901. doi:10.1088/0953-8984/27/43/435901.

[41] S.N. Gvasaliya, R.A. Cowley, L.I. Ivleva, S.G. Lushnikov, B. Roessli, A. Zheludev, Phase transition of the uniaxial disordered ferroelectric Sr0.61Ba0.39Nb2O6, J. Phys.-Condes. Matter. 26 (2014) 185901. doi:10.1088/0953-8984/26/18/185901.

[42] J.A. Bock, J.H. Chan, Y. Tsur, S. Trolier-McKinstry, C.A. Randall, The Effects of Low Oxygen Activity Conditions on the Phase Equilibria and Cation Occupancy of Strontium Barium Niobate, J. Am. Ceram. Soc. 99 (2016) 3435–3442. doi:10.1111/jace.14351.

[43] T.S. Chernaya, T.R. Volk, I.A. Verin, L.I. Ivleva, V.I. Simonov, Atomic structure

of $(Sr_{0.50}Ba_{0.50})Nb_2O_6$ single crystals in the series of $(Sr_xBa_{1-x})Nb_2O_6$ compounds, Crystallogr. Rep. 47 (2002) 213–216. doi:10.1134/1.1466494.

[44] M. Gao, S. Kapphan, S. Porcher, R. Pankrath, Experimental study of NIR absorption due to Nb^{4+} polarons in pure and Cr- or Ce-doped SBN crystals, J. Phys.-Condes. Matter. 11 (1999) 4913–4924. doi:10.1088/0953-8984/11/25/310.

[45] M. Melo, E.B. Araujo, A.P. Turygin, V.Y. Shur, A.L. Kholkin, Physical properties of strontium barium niobate thin films prepared by polymeric chemical method, Ferroelectrics. 496 (2016) 177–186. doi:10.1080/00150193.2016.1155035.

[46] M. Said, T.S. Velayutham, W.C. Gan, W.H. Abd Majid, The structural and electrical properties of $Sr_xBa_{(1-x)}Nb_2O_6$ (SBN) ceramic with varied composition, Ceram. Int. 41 (2015) 7119–7124. doi:10.1016/j.ceramint.2015.02.023.

[47] P.K. Patro, A.R. Kulkarni, C.S. Harendranath, Dielectric and ferroelectric behavior of SBN50 synthesized by solid-state route using different precursors, Ceram. Int. 30 (2004) 1405–1409. doi:10.1016/j.ceramint.2003.12.087.

[48] S. Hirano, T. Yogo, K. Kikuta, K. Ogiso, Preparation of Strontium Barium Niobate by Sol-Gel Method, J. Am. Ceram. Soc. 75 (1992) 1697–1700. doi:10.1111/j.1151-2916.1992.tb04251.x.

[49] S. Tanaka, T. Takahashi, K. Uematsu, Fabrication of transparent crystal-oriented polycrystalline strontium barium niobate ceramics for electro-optical application, J. Eur. Ceram. Soc. 34 (2014) 3723–3728. doi:10.1016/j.jeurceramsoc.2014.05.006.

[50] Y. Ebina, T. Higuchi, T. Hattori, T. Tsukamoto, Electronic structure in the valence band of *c*-axis oriented $Sr_{0.50}Ba_{0.50}Nb_2O_6$ thin film on $La_{0.05}Sr_{0.95}TiO_3$ substrate, Elsevier Science Bv, Amsterdam, 2006.

[51] S. Podlozhenov, H.A. Graetsch, J. Schneider, M. Ulex, M. Woehlecke, K. Betzler, Structure of strontium barium niobate $Sr_xBa_{1-x}Nb_2O_6$ (SBN) in the composition range 0.32 <= x <= 0.82, Acta Crystallogr. Sect. B-Struct. Sci. 62 (2006) 960–965. doi:10.1107/S0108768106038869.

[52] C.S. Dandeneau, Y. Yang, M.A. Olmstead, R.K. Bordia, F.S. Ohuchi, Polaronic conduction and Anderson localization in reduced strontium barium niobate, Appl. Phys. Lett. 107 (2015) 232901. doi:10.1063/1.4937435.

[53] R. Demirbilek, A.B. Kutsenko, R. Pankrath, S.E. Kapphan, Absorption spectroscopy and energy levels of rare earth impurity centres in $Sr_xBa_{1-x}Nb_2O_6$ crystals, Phys. Status Solidi B-Basic Solid State Phys. 246 (2009) 1306–1312. doi:10.1002/pssb.200844336.

[54] L. Yi, L. Jian, W. Chun-Lei, S. Wen-Bin, Z. Yuan-Hu, L. Ji-Chao, M. Liang-Mo, Thermoelectric properties of Sr 0.61 Ba 0.39 Nb 2 O 6− δ ceramics in different oxygen-reduction conditions, Chinese Phys. B. 24 (2015) 047201.

doi:10.1088/1674-1056/24/4/047201.
[55] G.A. Slack, New materials and performance limits for thermoelectric cooling, in: CRC Handbook of Thermoelectrics, CRC Press, 1995: pp. 407–440.
[56] T.M. Tritt, Thermoelectric Phenomena, Materials, and Applications, in: Annual Review of Materials Research, Annual Reviews, 2011: pp. 433–448.
[57] Y. Li, J. Liu, Z. Wang, Y. Zhou, C. Wang, J. Li, Y. Zhu, M. Li, L. Mei, Effects of fluorine doping on thermoelectric properties of Sr 0.61 Ba 0.39 Nb 2 O 6 ceramics, Phys. Scr. 90 (2015) 025801. doi:10.1088/0031-8949/90/2/025801.
[58] S.H. Kshirsagar, A.N. Tarale, S.R. Jigajeni, D.J. Salunkhe, S.B. Kulkarni, P.B. Joshi, Ferroelectric and Magnetodielectric Properties of Cobalt-Doped Sr (x) Ba1-x Nb2O6 Ceramics, J. Electron. Mater. 44 (2015) 2321–2330. doi:10.1007/s11664-015-3792-7.
[59] T.-T. Fang, H.-Y. Chung, C.-H. Lee, Defects, Structure Changes, and the Effect of Random Fields on the Displacement of Off-Center Ions in $Sr_{0.50}Ba_{0.50}Nb_2O_6$ Doped with Combinations of Ce and Cr, J. Am. Ceram. Soc. 93 (2010) 2339–2345. doi:10.1111/j.1551-2916.2010.03745.x.
[60] S.M. Kaczmarek, T. Tsuboi, A. Leniec, Y. Nakai, G. Leniec, M. Berkowski, W. Huang, Temperature dependence of PL and EPR spectra of $Sr_{0.33}Ba_{0.67}Nb_2O_6$: Cr (0.02 mol%) single crystals, J. Cryst. Growth. 401 (2014) 798–801. doi:10.1010/j.jcrysgro.2014.02.035.
[61] L.I. Ivleva, N.S. Kozlova, E.V. Zabelina, Study of the temperature dependence of the electrical conductivity in strontium-barium niobate crystals with different dopants, Crystallogr. Rep. 52 (2007) 328–331. doi:10.1134/S1063774507020277.
[62] K.P. Guzhakovskaya, A.I. Burkhanov, L.I. Ivleva, I.E. Tumanov, The Behavior of Current and Dielectric Response in SBN-75:Cr Single Crystal under Illumination Effect, Ferroelectrics. 469 (2014) 92–96. doi:10.1080/00150193.2014.948790.
[63] G.H. Olsen, S.M. Selbach, T. Grande, On the energetics of cation ordering in tungsten-bronze-type oxides, Phys. Chem. Chem. Phys. 17 (2015) 30343–30351. doi:10.1039/c5cp05119c.
[64] T.S. El-Shazly, W.M.I. Hassan, S.T.A. Rahim, N.K. Allam, Unravelling the interplay of dopant concentration and band structure engineering of monoclinic niobium pentoxide: A model photoanode for water splitting, Int. J. Hydrog. Energy. 40 (2015) 13867–13875. doi:10.1016/j.ijhydene.2015.08.056.
[65] R. Ottini, C. Tealdi, C. Tomasi, I.G. Tredici, A. Soffientini, U. Anselmi-Tamburini, P. Ghigna, G. Spinolo, Feasibility of electron and hole injection in heavily doped strontium barium niobate (SBN50) Sr0.5Ba0.5Nb2O6 for thermoelectric applications., J. Appl. Phys. 121 (n.d.) 085104.

doi:10.1063/1.4977102.
[66] L. Lutterotti, S. Matthies, H.-R. Wenk, MAUD: a friendly Java program for material analysis using diffraction, IUCr: Newsletter of the CPD. 21 (1999) 14–15.
[67] Atomistic Simulation Group, Materials Department of Imperial College, Database of Ionic Radii - http://abulafia.mt.ic.ac.uk/shannon/ptable.php, Database of Ionic Radii. (n.d.). http://abulafia.mt.ic.ac.uk/shannon/ptable.php (accessed May 12, 2016).
[68] F. D'Acapito, S. Colonna, S. Pascarelli, G. Antonioli, A. Balerna, A. Bazzini, F. Boscherini, F. Campolungo, G. Chini, G. Dalba, I. Davoli, P. Fornasini, R. Graziola, G. Licheri, F. Meneghini, C. Rocca, L. Sangiorgio, V. Sciarra, V. Tullio, S. Mobilio, GILDA Italian Beamline on BM08, ESRF Newsl. 30 (1998) 42–44.
[69] B. Ravel, M. Newville, ATHENA, ARTEMIS, HEPHAESTUS: data analysis for X-ray absorption spectroscopy using IFEFFIT, J Synchrotron Rad, J Synchrotron Radiat. 12 (2005) 537–541. doi:10.1107/S0909049505012719.
[70] N. Binsted, S.S. Hasnain, State-of-the-art analysis of whole X-ray absorption spectra, J. Synchrot. Radiat. 3 (1996) 185–196. doi:10.1107/S0909049596005651.
[71] T. Kolodiazhnyi, A. Petric, M. Niewczas, C. Bridges, A. Safa-Sefat, J.E. Greedan, Thermoelectric power, Hall effect, and mobility of n-type BaTiO3., Phys. Rev. B. 68 (2003) 085205.
[72] P.A. Cox, Transition Metal Oxides: An Introduction to Their Electronic Structure and Properties, Clarendon Press, Oxford, 1995.
[73] T. Hahn, INTERNATIONAL TABLES FOR CRYSTALLOGRAPHY, Springer, Dordrecht, The Netherlands, 2006.

Graphical Abstract

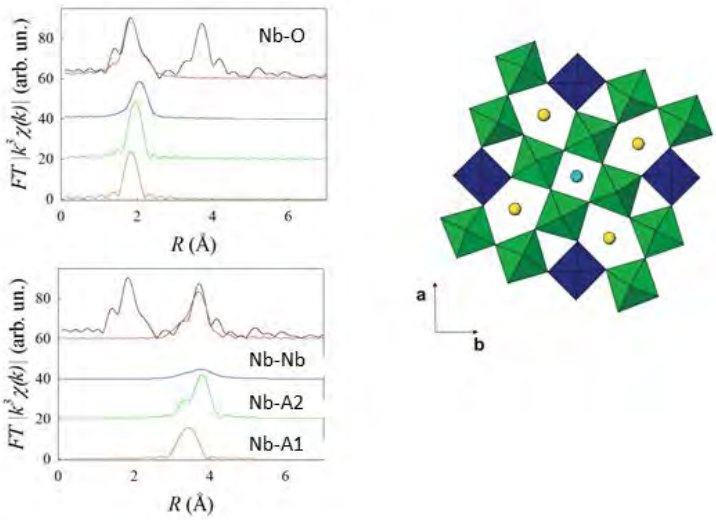

EXAFS Radial Distribution Function for Nb, and a projection of the SBN structure along the *c* axis. The two different sets of symmetry - equivalent Nb-O octahedra are marked in green and dark blue. Cyan and yellow spheres mark the A1 (occupied by Sr only) and A2 sites (occupied by both Sr and Ba).